Flow pattern in inner cores of double emulsion droplets

Shaohua MA,[1,2] Joseph M. SHERWOOD,[3,4] Wilhelm T. S. HUCK[1,5,*] and Stavroula BALABANI[3,*]

* Corresponding author: w.huck@science.ru.nl; s.balabani@ucl.ac.uk
1. Department of Chemistry, University of Cambridge, Cambridge CB2 1EW, UK
2. Department of Chemistry, University of Oxford, Oxford OX1 3TA, UK
3. Department of Mechanical Engineering, University College London, London WC1E 7JE, UK
4. Department of Bioengineering, Imperial College London, London SW7 2AZ, UK.
5. Radboud University Nijmegen, Institute for Molecules and Materials, Heyendaalseweg 135, 6525 AJ Nijmegen, The Netherlands.

Abstract The efficacy of applications of water-in-oil-in-water (w/o/w) double emulsions moving in microchannels is significantly impacted by the flow conditions in the inner aqueous cores. For example in the case of shear sensitive cells transported in the cores, high shear conditions may be deleterious. This study reports on the flow topology inside w/o/w cores determined by means of micro-particle image velocimetry (μPIV) and compares it to the flow in single water-in-oil (w/o) microdroplets with equal sizes moving in a rectangular microchannel. The multiphase flow system employed in the study had a viscosity ratio, λ, between oil and aqueous phase of the order of unity (λ = 0.8) and both single and compound droplets filled the channels. This configuration resulted in a weak recirculating flow inside the w/o single droplet: the measured flow field exhibited a uniform low velocity flow field in the central region surrounded by small regions of reversed flow near the channel walls. This flow topology was maintained in the inner cores of w/o/w double emulsions for intermediate capillary numbers (*Ca*) ranging from 10^{-3} to 10^{-2}, and core morphologies varying from large plug to pancake cores. The core morphology affected the magnitude and distribution of the velocity in the droplets. The similarity in the flow pattern results from the fact that inner cores were located at the back of the outer droplet in such a way that inner and outer interfaces were in contact for half of core surface area and separated by a thin lubricating film.

Keywords: Double Emulsion, Droplet, Microfluidics, Micro-Particle Image Velocimetry, Flow Topology

Introduction

Droplet-based microfluidics has been the subject of extensive research due to the wide ranging applications of this technology, as it minimises the volume and time scale required in micromanipulation by compartmentalising targets in droplets and isolating them in the continuous phase. Knowledge of the flow field inside the droplets is of paramount importance in order to tailor them to a specific application. W/o/w double emulsions have advantages over single w/o droplets in the formulation of complex microparticles (Nie et al., 2005; Gao et al., 2009) and giant polymersomes (Kim et al., 2013; Shum et al., 2008; Meng et al., 2005; Thiele et al., 2014), with application in controlled drug release (Rodríguez-García et al., 2011; Kim et al., 2009; Kim et al., 2011; LoPresti et al., 2009) as well as biomimetic cellular structures (Marguet et al., 2013; Marguet et al., 2012; Martino et al., 2012). High-throughput cell manipulation requires encapsulation at high speed, which can generate a harsh shear environment inside the droplets, potentially harming the viability of certain cells (Brouzes et al., 2009; Tasoglu et al., 2013). For example, strong shear forces originating from the hydrodynamic focusing effect that aligns the cell samples flowing through the nozzle into a single file flow have been found to cause physiological alterations and reduce fertilisation after sex sorting of sperm in flow cytometry (Leahy and Gadella, 2011; Rath et al., 2013; Mollet et al., 2008). Droplet screening offers a route to protect sperm cells against such external shear stresses in flow cytometry, on the condition that the droplet interior provides

a milder environment to the screened cells. However, w/o droplets are not compatible with commercial flow cytometry methods, such as fluorescence-activated cell sorting (FACS), owing to the fact that the carrier fluid in FACS is aqueous, whereas w/o droplets are carried by oil.

µPIV can be used to quantitatively characterize microscale flows (Lindken et al., 2009), including those in microdroplets and double emulsions. In recent years, it has been widely used to study the droplet flow topology of liquid-liquid systems in microfluidics (Malsch et al., 2008; Kinoshita et al., 2007; Prat et al., 2006; King et al., 2007; Miessner et al., 2008; Dore et al., 2012). However, to the best of our knowledge no µPIV study has been reported on the flow conditions in double emulsions, especially those in inner cores of w/o/w double emulsions that are of interest in flow cytometry applications.

The present study reports on the flow topology inside the aqueous inner cores of w/o/w double emulsions measured by µPIV. The double emulsions comprised an aqueous buffer, water and fluorinated oil phases (with surfactants added in selected phases) and moved in rectangular microchannels. The velocity field measured in the inner aqueous cores was compared to that found inside aqueous single droplets, of approximately same size, and *Ca* range (10^{-3} to 10^{-2}).

Experimental procedures

All chemicals were purchased from Sigma Aldrich Co. UK, unless noted otherwise and used without further purification. Deionised water was used in all aqueous phases. Microfluidic PDMS devices were fabricated by combined photo- and soft lithography (Xia and Whitesides, 1998). Detailed channel architectures were designed in AutoCAD (AutoDesk, USA). The microchannel geometry is shown in Figure 1a: a channel depth of 150 µm was achieved by spin-coating SU8 2025 (MicroChem, USA) at 75 µm onto a 3-inch silicon wafer (Compart Technology Ltd, UK) twice. The width of the channels was 100 µm upstream of the droplet formation nozzle and 200 µm downstream. The channel surface properties were modified by flushing the channel with 0.5% Trichloro (1*H*,1*H*,2*H*,2*H*-perfluorooctyl) silane in HFE7500 (297730-93-9, 3M, 0.77cSt). A high-precision syringe pump (Fusion 400, Chemyx Inc., USA) was used for the single droplet formation whereas for the double emulsions a combination of a syringe pump and pressure controlled system (Sherwood et al., 2012) was used.

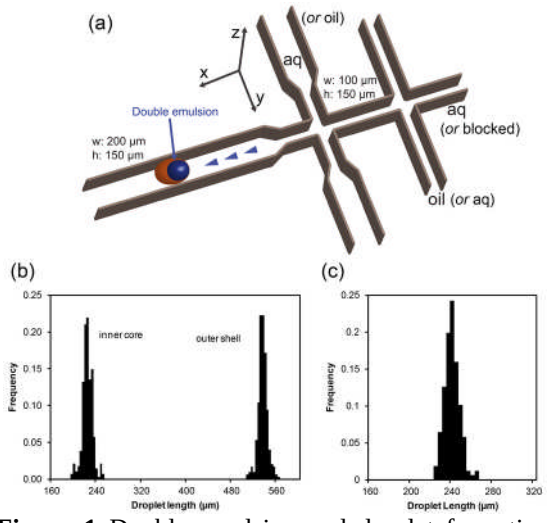

Figure 1 Double emulsion and droplet formation system. (a) 3D drawing of the microfluidic channel architecture. The channel had a fixed depth of 150 µm; the channel width was 150 µm in the formation region and 200 µm further downstream as illustrated. Single droplets were generated by blocking the innermost inlet channel. The long straight channel downstream of the 2nd nozzle, where droplet images were acquired was 200 µm wide and 20 mm long (b, c) Typical size distributions obtained by counting over 200 w/o/w double emulsions (b) and w/o single droplets (c) formed at a volume flow rate of (b) 1200 µl/hr and (c) 800 µl/hr, respectively.

The aqueous and the oil phases were injected independently into the microchannel. The inner aqueous fluid (1.0 M phosphate buffered saline (PBS), pH 7.4) formed w/o droplets at the first cross-junction by flow-focusing with the fluorinated oil HFE7500, and second emulsification of these droplets followed at the second cross-junction, generating

w/o/w double emulsions. The continuous phase was water, loaded with 1.5 wt% sodium dodecyl sulphate (SDS). The inner core was seeded with 1.1 µm Nile Red fluorescent tracing particles (FluoSphere F-8819, Invitrogen Inc., USA) at a concentration of 6×10^6 particles per ml before flow delivery. At this seeding concentration the particles were not found to affect the measured flow patterns. Single droplet formation was achieved in the same microfluidic device by blocking the innermost inlet channel; thus the PBS buffer and the oil phase were injected into the microfluidic channels independently from the two remaining inlets. The monodispersity of both double emulsions and single droplets were examined separately by measuring the length of over 200 imaged double emulsions and single droplets generated at fixed volume rates of individual phases. As both the double emulsions and single droplets completely filled the channel width, their length was considered sufficient to characterise their size distribution. Figures 1b and 1c show that both the double emulsion, including the inner core, and single droplet monodispersity are well established, satisfying thus the criteria for ensemble cross-correlation of the acquired image pairs during µPIV data processing.

A µPIV system developed by Sherwood *et al.* (Sherwood et al., 2014) was used for measurements of the flow field inside the droplets. A schematic of the system is shown in Figure 2a. The microfluidic device was mounted onto the stage of an inverted microscope (Leica DM ILM, Germany). The inner aqueous and oil phases were pumped into the microchannel from suitably sized syringes at various flow rates and the continuous aqueous phase in the double emulsions was perfused from a pressure controlled aqueous reservoir. The flow was illuminated by both a dual cavity Nd:YAG laser operating at 532 nm (New Wave, USA) and a microstrobe. The fluorescence light emitted by the tracing particles seeded in the flow passed through a 610/75nm dichroic mirror/filter cube.

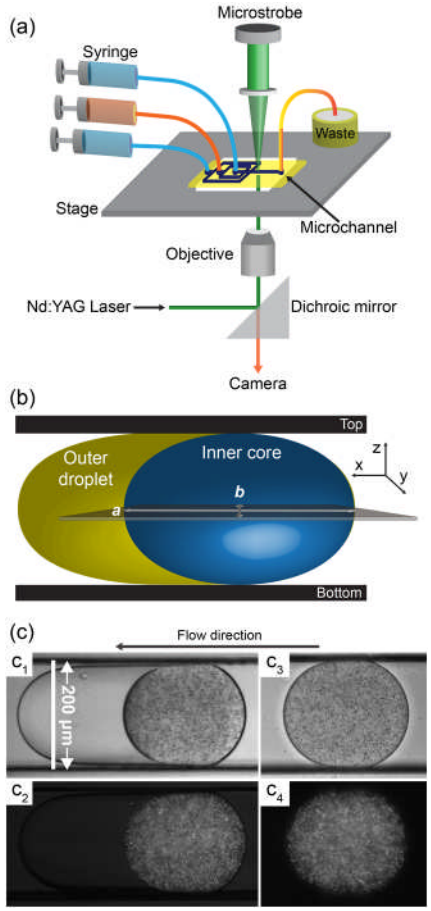

Figure 2 Image acquisition system. (a) Schematic of the µPIV setup comprised of the microfluidic device, the flow delivery system, the light sources, the microscope unit and the CCD camera. (b) Illustration of the mid-plane across the inner core where images were acquired. The dimensions of the inner core in *x*, *y* directions are noted as *a* and *b*, respectively. (c) Typical (c_1, c_3) bright-field and (c_2, c_4) fluorescent images of (c_1, c_2) w/o/w double emulsions and (c_3, c_4) w/o droplets explored in this paper.

Fluorescent and strobe images were acquired alternatively using a CCD (Hamamatsu, Japan) camera operating in double-frame mode at 6 Hz. A 10× (NA = 0.25) objective lens was used, resulting in a depth of field of 38 µm (Olsen and Adrian, 2000). Triggering and image acquisition were carried out via Labview (National Instrument, Texas, USA). Figure 2b illustrates the central focal planes, *i.e.* the mid-plane in the *z*- axis, where images

were acquired. Figure 2c shows typical bright-field and corresponding fluorescent images for a double emulsion (c_1, c_2) and a single droplet (c_3, c_4).

The centroids of individual droplets in selected fluorescent image pairs were calculated using Labview and overlapped to offset the droplet movement during the time delay, Δt, in order to cross-correlate the acquired images and obtain the droplet flow field in the reference frame of the moving droplet (Lagrangian frame).

Based on the monodispersity of double emulsions or single droplets, ensemble correlation (Delnoij et al., 1999) of 30 – 50 image pairs, using the open source software JPIV, was used. Outliers were identified by applying the normalised median test (Westerweel and Scarano, 2005) and replaced by the median of the surrounding vectors in the vector plots. The vector field was further smoothed with a 3 × 3 median filter (Raffel et al., 2007).

Ca was defined based on the velocity of the continuous phase, v_c, as

$$Ca = \mu_c v_c / \gamma$$

where μ_c is the viscosity of the continuous phase, and γ is the w/o interfacial tension. The velocity of the inner core of double emulsions and single droplets was determined from the strobe illuminated images by measuring the distance in pixels of the two images in each image pair, calibrating and dividing by Δt. The viscosity ratio of the aqueous phase against the oil phase is 0.80. As SDS exists at very low concentration in the outermost phase, we assume the viscosity is unaltered by the surfactant. The inner cores were found to be located at the rear of double emulsions, when the flow reached an equilibrium state, and did not move relative to the oil shell. The distortion resulting from the mismatch in the refractive indices of water (1.33, 20 °C) and HFE7500 (1.29, 20 °C) in the water droplets in HFE7500 was found to be negligible, according to a ray tracing methodology (Minor et al., 2007).

Results and Discussion

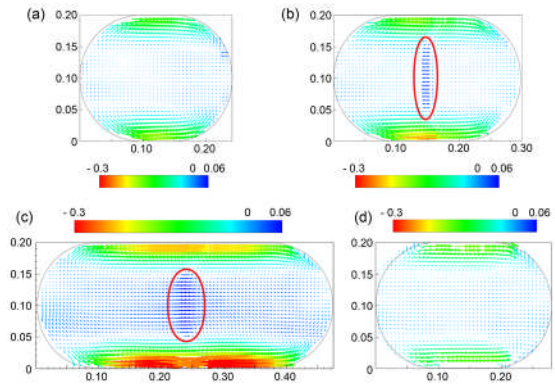

Figure 3 Velocity vector fields at the mid-planes of the inner cores of double emulsions. Core morphology varies from (a) a pancake core, (b) a small plug core, to (c) a large plug core. (d) A small single emulsion plug droplet. The velocity vectors are normalised by the droplet velocity, v_d. The red circles in (b) and (c) highlight the positive flow in the core centres. *Ca* are: (a) 1.6×10^{-3}; (b) 2.6×10^{-3}; (c) 5.2×10^{-3}; (d) 2.4×10^{-3}.

Figures 3a, b and c show vectors of the mid-plane velocities of w/o/w double emulsions with different sized inner cores. Figure 3d gives the measured vector plot of a w/o droplet plug of similar size to the droplet in the Figure 3b. The flow topology is similar in all cases: the central region exhibits low magnitude, near zero, velocities, accompanied by two regions of relative high velocity, reversed flow (*i.e.* opposite to the droplet motion) on both sides of the centreline and close to the w/o interfaces. The flow pattern in the interior of the single droplet shown in Figure 3d differs from the established recirculating pattern reported in most studies; this is due to the viscosity ratio between the oil and water phase (0.80) as reported in our previous study (Ma et al., 2014), which in combination with the boundary conditions results in less pronounced flow reversal in the interior of the droplet. Interestingly, the same flow topology is observed in the inner cores of w/o/w double emulsions. However, some *positive* net flow, highlighted in the red region in Figures 3b and 3c, can be observed in the central region of the inner cores which is more

pronounced in plug cores than pancake and spherical cores, whereas the corresponding region in single droplets exhibits negligible velocity in that region.

A comparison of the velocity field measured inside inner cores of different morphologies (aspect ratios) is given in Figure 4. The left and right columns represent the axial and transverse velocity components normalised by the inner droplet (core) velocity v_d, $\bar{u}/v_d$ and $\bar{v}/v_d$, respectively. As the inner core is pushed to the rear of the shell by drag, it is assumed that there is no relative movement between the core and double emulsion itself. Qualitatively, the distributions of the two velocity components are identical among cores with aspect ratios a/b ranging from 1 to 2.5. It was found in this study that the topology persisted for Ca ranging from 10^{-3} to 10^{-2}. However the normalised velocity magnitude decreases with core aspect ratio, with the larger plug cores exhibiting higher velocities, than pancake cores, particularly in the axial component.

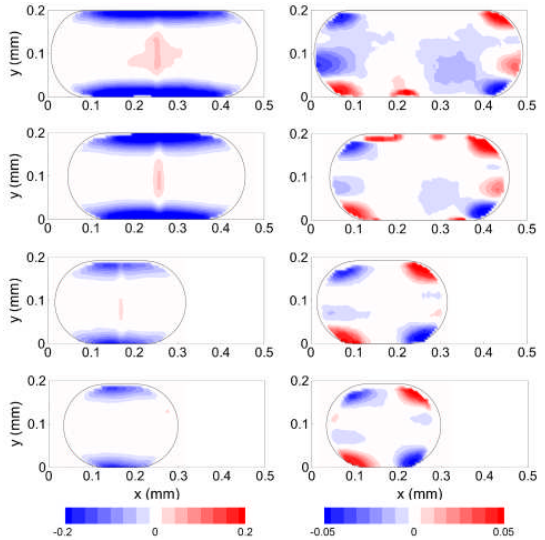

Figure 4 Contours of normalised velocity components measured in inner cores of w/o/w double emulsions with different aspect ratios. The velocity components are normalised by the inner core velocity, *i.e.* $\bar{u}/v_d$ (*left* column) and $\bar{v}/v_d$ (*right* column).

Figure 5 compares the distributions of axial and transverse velocities ($\bar{u}/v_d$ and $\bar{v}/v_d$) between an inner core and a single droplet of approximately equal size. The distributions of both $\bar{u}/v_d$ and $\bar{v}/v_d$ show some similarities, and the velocity magnitudes are comparable. This similarity can be explained as follows. The inner core is always located in the rear of the double emulsion, regardless of the size, with over half area of the w/o interface in close contact with the oil-in-water (o/w) interface (the interface between the middle oil phase with the continuous aqueous phase). A thin lubricating layer exists between the two interfaces which is only slightly more viscous than the aqueous phase (λ = 0.8) (Terwagne, et al. 2010). Boundary conditions lead to continuity of velocity across both interfaces, resulting in reduced lubricating effect by the oil layer. Though the w/o interface is not totally coincident with the o/w interface in the double emulsions, the common part appears to primarily dictate the pattern observed. The regions along the interface not in contact with channel walls experience zero or negligible velocities.

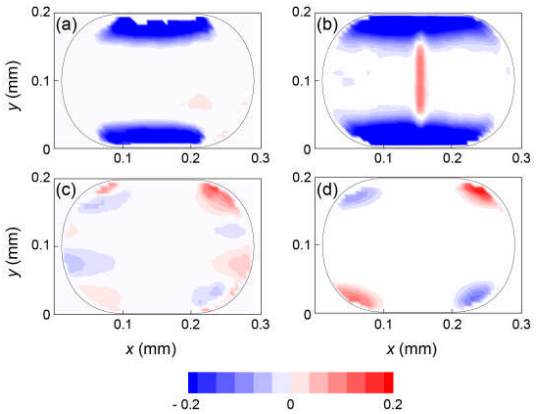

Figure 5 Contours of the normalised velocity components, $\bar{u}/v_d$ and $\bar{v}/v_d$, of (a, c) a single droplet and (b, d) the inner core of a double emulsion. The inner w/o core is of the similar size as the single o/w droplet.

It is clear from the above that the core geometry and Ca (in the range considered), do not significantly affect the flow topology, but only the magnitude of flow velocities, as shown in Figures 3 and 4. Therefore we can conclude that the inner cores of w/o/w double emulsions, in the current eccentric configuration, exhibit

similar flow conditions as equally sized w/o single droplets. Furthermore, it is reasonable to assume symmetry and expect the core flow topology to vary accordingly in the *yz* plane, and conclude that the central region of the inner cores exhibits lower velocities, whereas the regions near the channel boundaries have higher magnitude and reversed velocity flows.

Conclusion

The flow field in the inner cores of w/o/w double emulsions moving in a rectangular microchannel was studied by means of µPIV and an identical flow topology to that of single droplets was observed at moderate *Ca*, 10^{-3} to 10^{-2}. In the studied systems of single droplet and inner core of double emulsion, low velocity flow was found in the central region and high velocity reversed flow was confined along the interface unlike the typical recirculating pattern reported in previous studies; this was the result of the viscosity ratio employed in the present study. The study shows that *Ca* and core (droplet) morphology do not affect the flow topology but affect the flow velocity magnitude. The inner cores exhibit analogous flow topologies and velocity magnitudes with equally sized single droplets composed of the inner core and middle oil shell of double emulsions. The results indicate that double emulsions are suitable candidates to substitute single droplets in flow cytometry to protect the screened items and are compatible with the commercial flow cytometry systems. Thus potentially w/o/w double emulsions can protect screened sperm cells from harsh shear environment in FACS and achieve better cell viability recovery rate.

Acknowledgement

SM acknowledges the financial support provided by the CSC Cambridge Scholarship throughout his PhD studies. SB would like to thank Dantec Dynamics for the loan of the laser used in this study. Finally the authors wish to thank Dr Peter Vennemann for providing the free PIV analysis software JPIV (http://www.jpiv.vennemann-online.de/).

Bibliography

Brouzes, E., Medkova, M., Savenelli, N., Marran, D., Twardowski, M., Hutchison, J.B., Rothberg, J.M., Link, D.R., Perrimon, N., Samuels, M.L., 2009. Droplet microfluidic technology for single-cell high-throughput screening. Proc. Natl. Acad. Sci. U. S. A. 106, 14195–200. doi:10.1073/pnas.0903542106

Delnoij, E., Westerweel, J., Deen, N.G., Kuipers, J. A. M., van Swaaij, W.P.M., 1999. Ensemble correlation PIV applied to bubble plumes rising in a bubble column. Chem. Eng. Sci. 54, 5159–5171. doi:10.1016/S0009-2509(99)00233-X

Dore, V., Tsaoulidis, D., Angeli, P., 2012. Mixing patterns in water plugs during water/ionic liquid segmented flow in microchannels. Chem. Eng. Sci. 80, 334–341. doi:10.1016/j.ces.2012.06.030

Gao, F., Su, Z.-G., Wang, P., Ma, G.-H., 2009. Double emulsion templated microcapsules with single hollow cavities and thickness-controllable shells. Langmuir 25, 3832–8. doi:10.1021/la804173b

Kim, K.T., Cornelissen, J.J.L.M., Nolte, R.J.M., van Hest, J.C.M., 2009. A Polymersome Nanoreactor with Controllable Permeability Induced by Stimuli-Responsive Block Copolymers. Adv. Mater. 21, 2787–2791. doi:10.1002/adma.200900300

Kim, S.-H., Nam, J., Kim, J.W., Kim, D.-H., Han, S.-H., Weitz, D.A., 2013. Formation of polymersomes with double bilayers templated by quadruple emulsions. Lab Chip 13, 1351–6. doi:10.1039/c3lc41112e

Kim, S.-H., Shum, H.C., Kim, J.W., Cho, J.-C., Weitz, D.A., 2011. Multiple polymersomes for programmed release of multiple components. J. Am. Chem. Soc. 133, 15165–71. doi:10.1021/ja205687k

King, C., Walsh, E., Grimes, R., 2007. PIV measurements of flow within plugs in a microchannel. Microfluid. Nanofluidics 3, 463–472. doi:10.1007/s10404-006-0139-y

Kinoshita, H., Kaneda, S., Fujii, T., Oshima, M., 2007. Three-dimensional measurement and visualization of internal flow of a moving droplet using confocal micro-PIV. Lab Chip 7, 338–46. doi:10.1039/b617391h

Leahy, T., Gadella, B.M., 2011. Sperm surface changes and physiological consequences induced by sperm handling and storage.

Reproduction 142, 759–78. doi:10.1530/REP-11-0310

Lindken, R., Rossi, M., Grosse, S., Westerweel, J., 2009. Micro-Particle Image Velocimetry (microPIV): recent developments, applications, and guidelines. Lab Chip 9, 2551–67. doi:10.1039/b906558j

LoPresti, C., Lomas, H., Massignani, M., Smart, T., Battaglia, G., 2009. Polymersomes: nature inspired nanometer sized compartments. J. Mater. Chem. 19, 3576. doi:10.1039/b818869f

Ma, S., Sherwood, J.M., Huck, T.S., Balabani, S., 2014. On the flow topology inside droplets moving in rectangular microchannels. Lab Chip. doi:10.1039/b000000x (accepted)

Malsch, D., Kielpinski, M., Merthan, R., Albert, J., Mayer, G., Köhler, J.M., Süße, H., Stahl, M., Henkel, T., 2008. µPIV-Analysis of Taylor flow in micro channels. Chem. Eng. J. 135S, S166–S172.

Marguet, M., Bonduelle, C., Lecommandoux, S., 2013. Multicompartmentalized polymeric systems: towards biomimetic cellular structure and function. Chem. Soc. Rev. 42, 512–29. doi:10.1039/c2cs35312a

Marguet, M., Edembe, L., Lecommandoux, S., 2012. Polymersomes in Polymersomes: Multiple Loading and Permeability Control. Angew. Chemie 124, 1199–1202. doi:10.1002/ange.201106410

Martino, C., Kim, S.-H., Horsfall, L., Abbaspourrad, A., Rosser, S.J., Cooper, J., Weitz, D. a, 2012. Protein expression, aggregation, and triggered release from polymersomes as artificial cell-like structures. Angew. Chem. Int. Ed. Engl. 51, 6416–20. doi:10.1002/anie.201201443

Meng, F., Engbers, G.H.M., Feijen, J., 2005. Biodegradable polymersomes as a basis for artificial cells: encapsulation, release and targeting. J. Control. Release 101, 187–98. doi:10.1016/j.jconrel.2004.09.026

Miessner, U., Lindken, R., Westerweel, J., 2008. 3D - Velocity measurements in microscopic two-phase flows by means of micro PIV, in: 14th Int Symp on Applications of Laser Techniques to Fluid Mechanics. pp. 7–10.

Minor, G., Oshkai, P., Djilali, N., 2007. Optical distortion correction for liquid droplet visualization using the ray tracing method: further considerations. Meas. Sci. Technol. 18, L23–L28. doi:10.1088/0957-0233/18/11/L01

Mollet, M., Godoy-Silva, R., Berdugo, C., Chalmers, J.J., 2008. Computer simulations of the energy dissipation rate in a fluorescence-activated cell sorter: Implications to cells. Biotechnol. Bioeng. 100, 260–72. doi:10.1002/bit.21762

Nie, Z., Xu, S., Seo, M., Lewis, P.C., Kumacheva, E., 2005. Polymer particles with various shapes and morphologies produced in continuous microfluidic reactors. J. Am. Chem. Soc. 127, 8058–63. doi:10.1021/ja042494w

Olsen, M.G., Adrian, R.J., 2000. Out-of-focus effects on particle image visibility and correlation in microscopic particle image velocimetry. Exp. Fluids 29, S166–S174. doi:10.1007/s003480070018

Prat, L., Gourdon, C., Sarrazin, F., Loubie, K., Bonometti, T., Magnaudet, J., 2006. Experimental and Numerical Study of Droplets Hydrodynamics in Microchannels. AIChE J. 52, 4061–4070. doi:10.1002/aic

Raffel, M., Willert, C.E., Wereley, S.T., Kompenhans, J., 2007. Particle Image Velocimetry: a practical guide, 2nd ed. Springer.

Rath, D., Barcikowski, S., Graaf, S. De, Garrels, W., Grossfeld, R., Klein, S., Knabe, W., Knorr, C., Kues, W., Meyer, H., Michl, J., Rehbock, C., Taylor, U., Washausen, S., de Graaf, S., Moench-Tegeder, G., 2013. Sex selection of sperm in farm animals: status report and developmental prospects. Reproduction 145, R15–30. doi:10.1530/REP-12-0151

Rodríguez-García, R., Mell, M., López-Montero, I., Netzel, J., Hellweg, T., Monroy, F., 2011. Polymersomes: smart vesicles of tunable rigidity and permeability. Soft Matter 7, 1532. doi:10.1039/c0sm00823k

Sherwood, J.M., Dusting, J., Kaliviotis, E., Balabani, S., 2012. The effect of red blood cell aggregation on velocity and cell-depleted layer characteristics of blood in a bifurcating microchannel. Biomicrofluidics 6, 024119. doi:10.1063/1.4717755

Sherwood, J.M., Kaliviotis, E., Dusting, J., Balabani, S., 2014. Hematocrit, viscosity and velocity distributions of aggregating and non-aggregating blood in a bifurcating microchannel. Biomech. Model. Mechanobiol. 13, 259–73. doi:10.1007/s10237-012-0449-9

Shum, H.C., Kim, J.-W., Weitz, D.A., 2008. Microfluidic fabrication of monodisperse biocompatible and biodegradable polymersomes with controlled permeability. J. Am. Chem. Soc. 130, 9543–9. doi:10.1021/ja802157y

Tasoglu, S., Gurkan, U.A., Wang, S., Demirci, U., 2013. Manipulating biological agents and cells in micro-scale volumes for applications in medicine. Chem. Soc. Rev. 42, 5788–808. doi:10.1039/c3cs60042d

Terwagne, D., Gilet, T., Vandewalle, N., Dorbolo, S., 2010. From a bouncing compound drop to

a double emulsion. Langmuir 2010, 11680–11685. doi: 10.1021/la101096q

Thiele, J., Chokkalingam, V., Ma, S., Wilson, D. A., Huck, W.T.S., 2014. Vesicle budding from polymersomes templated by microfluidically prepared double emulsions. Mater. Horizons 1, 96–101. doi:10.1039/c3mh00043e

Westerweel, J., Scarano, F., 2005. Universal outlier detection for PIV data. Exp. Fluids 39, 1096–1100. doi:10.1007/s00348-005-0016-6

Xia, Y., Whitesides, G.M., 1998. Soft Lithography. Annu. Rev. Mater. Sci. 28, 153–184. doi:10.1146/annurev.matsci.28.1.153